# The influence of waves on the tidal kinetic energy resource at a tidal stream energy site

Nicolas Guillou, Georges Chapalain, Simon P. Neill

# The influence of waves on the tidal kinetic energy ressource at a tidal stream energy site

by

Nicolas Guillou, Georges Chapalain and Simon P. Neill

Applied Energy
2016, Volume 180, pp. 402-415
http://dx.doi.org/10.1016/j.apenergy.2016.07.070

# The influence of waves on the tidal kinetic energy resource at a tidal stream energy site.

Nicolas Guillou[a,*], Georges Chapalain[a], Simon P. Neill[b]

[a]*Laboratoire de Génie Côtier et Environnement (LGCE), Cerema/DTecEMF/DS, 155 rue Pierre Bouguer Technopôle Brest-Iroise - BP 5 - 29280 Plouzané, France*
[b]*School of Ocean Sciences, Bangor University, Menai Bridge, UK*

**Abstract**

Successful deployment of tidal energy converters relies on access to accurate and high resolution numerical assessments of available tidal stream power. However, since suitable tidal stream sites are located in relatively shallow waters of the continental shelf where tidal currents are enhanced, tidal energy converters may experience effects of wind-generated surface-gravity waves. Waves may thus influence tidal currents, and associated kinetic energy, through two non-linear processes: the interaction of wave and current bottom boundary layers, and the generation of wave-induced currents. Here, we develop a three-dimensional tidal circulation model coupled with a phase-averaged wave model to quantify the impact of the waves on the tidal kinetic energy resource of the Fromveur Strait (western Brittany) - a region that has been identified with strong potential for tidal array development. Numerical results are compared with in-situ observations of wave parameters (significant wave height, peak period and mean wave direction) and current amplitude and direction 10 m above the seabed (the assumed technology hub height for this region). The introduction of waves is found to improve predictions of tidal stream power at 10 m above the seabed at the measurement site in the Strait, reducing kinetic energy by up to 9 % during storm conditions. Synoptic effects of wave radiation stresses and enhanced bottom friction are more specifically identified at the scale of the Strait. Waves contribute to a slight increase in the spatial gradient of available mean tidal stream potential between the north-western area and the south-eastern part of the Strait. At the scale of the region within the Strait that has been identified for tidal stream array development, the available mean spring tidal stream potential is furthermore reduced by 12 % during extreme waves conditions. Isolated effects of wave radiation stresses and enhanced bottom friction lead to a reduction in spring tidal potential of 7.8 and 5.3 %, respectively. It is therefore suggested that models used for tidal resource assessment consider the effect of waves in appropriately wave-exposed regions.

*Keywords:* marine renewable energy, TELEMAC 3D, TOMAWAC, unstructured grid, wave-current interaction, Sea of Iroise

*Corresponding author
*Email addresses:* nicolas.guillou@cerema.fr (Nicolas Guillou ), georges.chapalain@cerema.fr (Georges Chapalain), s.p.neill@bangor.ac.uk (Simon P. Neill)

## 1. Introduction

Among the different sources of marine renewable energy, the kinetic power of tidal currents has, because of its astronomical origin, the major advantages of being predictable. In addition to their predictability, tidal stream devices, which generally take the form of horizontal axis turbines [1], have the advantage of a reduced visual impact which is helpful for public acceptance, particularly by coastal users and communities. Tidal stream technologies are thus developing very rapidly with several projects in the process of pre-commercial full-scale testing, including the twin rotor SeaGen device in Strangford Lough (Northern Ireland), the Andritz Hydro turbine off Kvalsund (Norway), the OpenHydro turbines off Paimpol-Bréhat (France), or the Sabella device near the isle of Ushant (France) [2]. Successful device deployment relies however on access to accurate and refined assessments of available tidal stream power. Numerical modelling tools are most of the time retained for the site selection process at the scale of continental shelves [3, 4] or locations identified for array implementation [5, 6, 7, 8]. However, whereas model predictions provide developers with key information for optimizing design and implementation of tidal energy converters [9], influences of meteorological forcings such as wind-generated surface-gravity waves on available tidal stream power are rarely considered in such studies.

Waves may however significantly impact tidal currents [10] and associated kinetic energy through two well-known major non-linear processes: interaction of wave and current bottom boundary layers [11], and the generation of wave-driven currents [12]. An increase in the apparent bottom friction felt by currents above the wave boundary layer may thus lead to a significant reduction of near-bottom velocity by up to 20 % during storm events [13]. The additional forcing of waves in regions of wave breaking creates radiation stress gradients, which may drive strong currents and modulate tidal circulations [14]. As tidal power density varies with the cube of velocity, more significant effects are expected on available tidal kinetic energy. Taking into account the variability of wave power over exposed continental shelves [15, 16, 17], waves may finally significantly affect variability and predictability of tidal stream power.

Nevertheless, whereas numerous numerical investigations have focused on the effects of waves on near-bottom tidal currents to improve predictions of hydrodynamic components and associated transport of sediment, temperature and salinity [18, 19, 20], little effort has been devoted to wave-induced variations of available tidal kinetic energy resource. In the field of marine renewable energy, much more effort has been invested in characterising fatigue and loading induced by waves upon devices, focusing on potential failure and reduced performance [21, 22, 23, 24] or investigating the effect of tidal currents on wave power [25, 26, 27]. The only major studies on this topic have been conducted by Lewis et al. [28] and Hashemi et al. [29]. Nevertheless, whereas Lewis et al. [28] exhibited a reduction of the theoretical tidal resource by 10 % for every metre increase in wave height, their numerical investigation was applied to an idealized headland case study, parameterised by the typical tide and wave conditions expected at tidal stream energy sites. A real application was performed by Hashemi et al. [29] to the planned tidal stream array off the north-western coast of Anglesey (UK) exhibiting a reduction in tidal stream power by 20 % for extreme winter waves. But predictions were established relying on depth-averaged circulation models, neglecting the complex three-dimensional (3D) tidal circulation associated with tidal flow separation in the wake of islands [30].

While models' performances were assessed against in-situ observations, improvements of numerical predictions reached by the integration of waves effects were disregarded.

The present study extends numerical investigations of waves effects on available tidal kinetic energy relying on (1) a 3D tidal circulation model applied to a real planned tidal stream array, and (2) in-situ observations of hydrodynamic components. A method is proposed for the coupling between a 3D circulation model and a phase-averaged wave model focusing on isolated or combined effects of wave radiation stresses and enhanced bottom friction. Numerical results are compared with in-situ measurements, which confirms improved performances in predictions of tidal stream power by the integration of waves effects. Besides an evaluation of this numerical method of broader interest for applications in wave-exposed regions, the present investigation quantifies the temporal and spatial effects of waves on tidal kinetic energy providing a first detailed analysis of the complex interactions between tidal currents, waves-driven circulation and modified bottom friction. These results promote finally the inclusion of waves effects for a refined assessment of the variability of tidal stream power in locations identified for array implementation.

The site of application is the Fromveur Strait off western Brittany (Fig. 1) considered, after the Alderney Race in the English Channel, to be the second largest French tidal stream resource, with a potential power estimated between 300 and 500 MW (section 2.1). Models predictions are evaluated against available observations of wave parameters (significant wave height, peak period and mean wave direction) and current amplitude and direction 10 m above the seabed (the assumed technology hub height for the region considered) (section 2.2). The modelling approach is based on a high-resolution 3D circulation model modified for coupling with simulations generated by a phase-averaged wave model (sections 2.3 and 2.4). The comparison between predictions and in-situ observations (section 3.1) exhibits the local and synoptic effects of waves on available tidal kinetic energy resource over a spring-neap cycle (section 3.2). A detailed analysis of these predictions is finally conducted for stationary offshore wave conditions quantifying the modulations of tidal stream power for both mean and extreme events (section 3.3).

Table 1: Description of wave and current measurement campaigns.

| Station number | Coordinates Lon. | Coordinates Lat. | Water depths (m) | Measurement campaigns |
|---|---|---|---|---|
| ADCP site | 5.036 $^{o}$ W | 48.449 $^{o}$ N | 53 | 19/03/1993 $\rightarrow$ 02/04/1993 |
| Deep wave buoy | 4.960 $^{o}$ W | 48.290 $^{o}$ N | 60 | 01/11/2012 $\rightarrow$ 30/11/2012 |
| Shallow wave buoy | 5.027 $^{o}$ W | 48.428 $^{o}$ N | 25 | 01/11/2012 $\rightarrow$ 30/11/2012 |

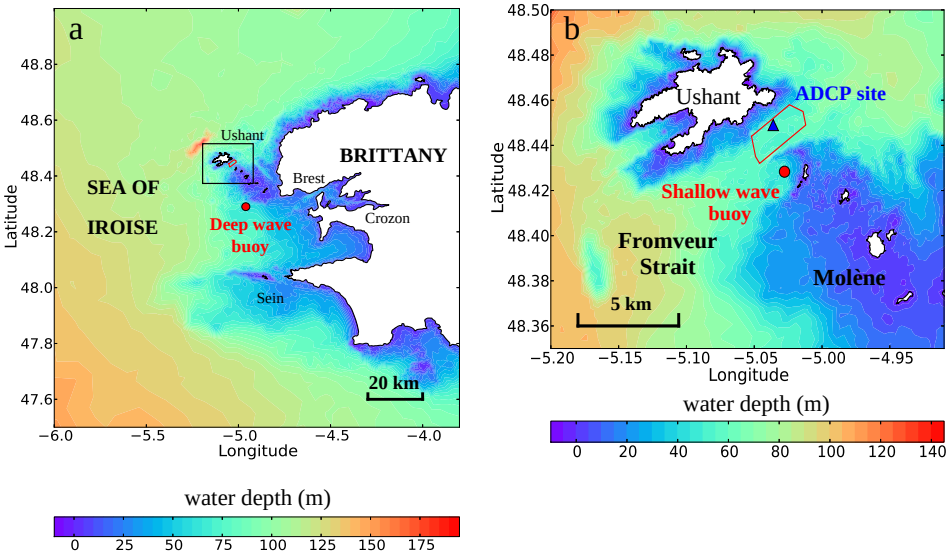


Figure 1: Bathymetry of (a) the western extent of Brittany, and (b) the Fromveur Strait with locations of available measurements points (● for wave buoys, ▲ for current meters). The red line in the Fromveur Strait delimits the region of interest for implementation of tidal stream devices. Water depth is relative to mean sea level.

Table 2: Nomenclature.

| Symbol | Description |
|---|---|
| $d$ | Total water depth (m) |
| $E$ | Directional spectrum of variance density (kg $s^{-1}$ $rd^{-1}$) |
| $F_x$, $F_y$ | Wave induced forces (m $s^{-2}$) |
| $f_\omega$ | Wave friction factor (-) |
| $g$ | Acceleration due to gravity ( $m\,s^{-2}$) |
| $H_s$ | Significant wave height (m) |
| $N$ | Wave action density function ($m^2$ $s^2$ $rd^{-1}$) |
| $P$ | Tidal stream energy per unit area ( $W\,m^{-2}$) |
| $S_{xx}$, $S_{xy}$, $S_{yy}$, $S_{yx}$ | Components of the radiation stress tensor ($m^3$ $s^{-2}$) |
| R | Pearson's correlation coefficient (-) |
| RE | Index of agreement (-) |
| $T_p$ | Peak wave period (s) |
| $u$ | Amplitude of the horizontal current component ( $m\,s^{-1}$) |
| $U_\omega$ | Wave bottom orbital velocity ( $m\,s^{-1}$) |
| $u_{*c}$ | Shear velocity arising from the current ( $m\,s^{-1}$) |
| $u_{*c\omega}$ | Total wave and current friction velocity ( $m\,s^{-1}$) |
| $u_{*\omega}$ | Shear velocity arising from the wave ( $m\,s^{-1}$) |
| $z_0$ | Bottom roughness parameter (m) |
| $z_{0,b\omega}$ | Apparent bottom roughness parameter (m) |
| $\delta_\omega$ | Thickness of the wave boundary layer (m) |
| $\rho$ | Water density ( $kg\,m^{-3}$) |
| $\sigma_\omega$ | Intrinsic wave frequency ($s^{-1}$) |
| $\tau_c$ | Current-induced bed shear stress ( $N\,m^{-2}$) |
| $\tau_{c\omega}$ | Total wave and current bed shear stress ( $N\,m^{-2}$) |
| $\tau_\omega$ | Wave-induced bed shear stress ( $N\,m^{-2}$) |
| $\phi_{c\omega}$ | Angle between wave and current directions (rd) |
| $\omega$ | Wave frequency ($s^{-1}$) |

## 2. Materials and methods

### *2.1. Study site*

Separating the isle of Ushant from the Molène archipelago, the Fromveur Strait has a width of 2 km and a mean water depth of 50 m. The seabed is mainly composed of rock and gravel deposits, complemented by surrounding sand in nearshore areas, and the presence of offshore sand banks of Ushant and the Four [31]. Considered as one of the leading French tidal stream sites, the Fromveur Strait is characterised by tidal ranges of up to 7 m during spring conditions and strong tidal flows, with annual averaged and maximum velocities of 1.5 and 4.0 $\mathrm{m\,s^{-1}}$, respectively [32] (Fig. 2). The surrounding area is characterised by clockwise rotating currents as a result of tidal wave propagation along the French Atlantic coast from the Bay of Biscay in the south towards the English Channel in the north-east. The detailed observation-based study conducted by Thiébaut et al. [33] highlighted furthermore strong tidal flow asymmetry in the Strait, with (1) a northeastern flood-dominated sector, and (2) a southward ebb dominated region separated by a region of tidal flow symmetry. Whereas density stratification effects are present in spring and summer due to the generation of offshore and nearshore thermal fronts [18], there are minimal density effects on the tidal currents within the Fromveur Strait itself [34]. Despite the shelter provided by the isle of Ushant, the Strait experiences, due to current-induced refraction [34], strong incoming waves from north-east and south-west directions, with average and maximum significant heights of around 1.5 and 5.0 m, respectively [16] (e.g. Fig. 2b).

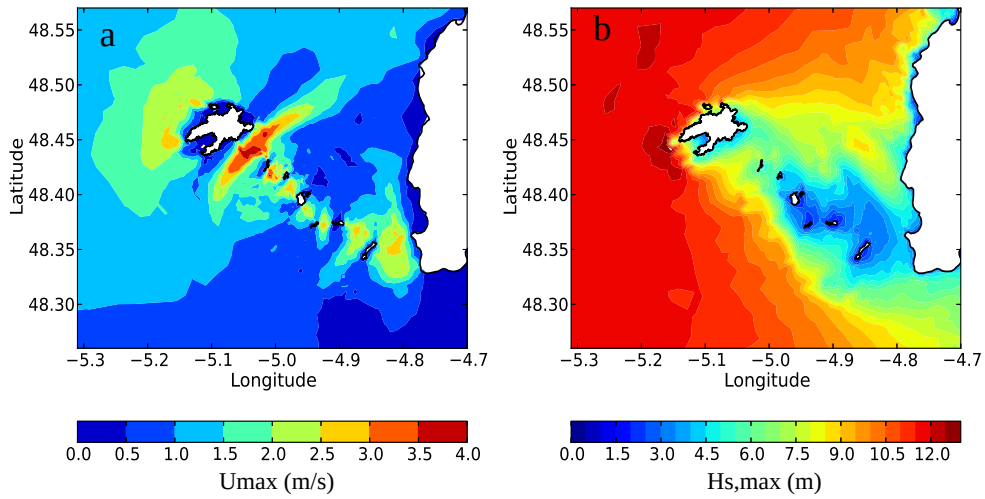


Figure 2: Predicted maximum (a) spring depth-averaged current, and (b) significant wave height over the period 2004-2011 in the Fromveur Strait [adapted from 16].

Power extraction from this site represents a promising alternative for meeting electricity demand in the isles of Ushant and Molène, reducing reliance on a fossil fuel power station. The French government has thus recently identified a restricted area of interest

of 4 km$^2$ for the implementation of tidal stream arrays in the Strait (Fig. 1-b). Accordingly, the French company Sabella SAS is currently testing a horizontal axis tidal turbine known as Sabella D10 in this area [35]. The device of 450 tonnes, deployed in 55 m water depth in the centre of the Strait, has a base of 20 m $\times$ 20 m along horizontal dimensions, a height of 17 m, and a rotor diameter of 10 m [36]. Recently connected to the grid on the isle of Ushant, the tidal turbine aims to achieve a rated power output of 0.5 MW.

### *2.2. In-situ measurements*

Available data used in this study consists of (1) current observations acquired by the SHOM ("Service Hydrographique et Océanographique de la Marine") in the Fromveur Strait (ADCP site) and (2) wave buoy measurements from the French CANDHIS database ("Centre d'Archivage National de Données de Houle In Situ", Cerema) (Fig. 1-b and Table 1). Current measurements were obtained with a 600 kHz RDI ADCP (Acoustic Doppler Current Profiler) deployed in a mean water depth of 53 m during spring and neap tidal conditions, from 19 March to 2 April 1993. The ADCP data are available in 2 m bins distributed throughout the water column from 6 to 52 m below the free surface. Taking into account difficulties associated with observations of tidal currents in the Fromveur Strait, in-situ data acquired by the SHOM constitute a unique opportunity to investigate the performance of a tidal circulation model in this area. Nevertheless, the wave measurements (November 2012) do not cover the same period as ADCP observations. These two periods will thus be selected for evaluating model predictions in the Fromveur Strait.

### *2.3. Numerical models*

The numerical approach is based on the finite-element modelling system TELEMAC (version 6p3) [37, 38] developed by the laboratory LNHE ("Laboratoire National d'Hydraulique et Environnement") of the French company EDF ("Electricité De France"). The simulation of hydrodynamic processes is based on the coupling between (1) the 3D circulation model TELEMAC 3D [39], and (2) the phase-averaged spectral wave model TOMAWAC [40]. Following methods adopted by Guillou and Chapalain [18] and Hashemi et al. [29] for computing wave and current interactions with TELEMAC, the coupling procedure is restricted to (1) modifications of the wave field due to time-varying water depths and currents, effects of (2) wave-driven currents, and (3) enhanced bottom friction resulting from wave-current interactions in the bottom boundary layer. The default versions of TELEMAC 3D and TOMAWAC have been modified to integrate these three processes. The description of the numerical models focuses on these modifications.

#### *2.3.1. TOMAWAC*

TOMAWAC solves the evolution of the wave action density $N = E/(\rho g \sigma_\omega)$, where $E$ is the directional spectrum of variance density, $\sigma_\omega$ is the intrinsic frequency, $\rho$ is the water density, and $g$ is the acceleration due to gravity. This evolution is computed with the time-dependent spectral action balance equation [41], expressing the conservation of action density according to different source and sink terms which generate, dissipate, or redistribute wave energy. These terms include deep and shallow water processes such as wave growth by wind, non-linear quadruplet and triad wave-wave interactions, energy dissipation by whitecapping, bottom friction, and depth-induced breaking. Parameterisations adopted for non-linear wave-wave interactions and depth-induced breaking are

taken from Guillou [42]. Energy dissipation by bottom friction is evaluated with the empirical constant value of bottom-friction coefficient suggested by Hasselmann et al. [43]. Wave growth by wind is described by the exponential term proposed by Komen et al. [44], while wave energy dissipation by whitecapping is formulated with the saturation-based model of van der Westhuysen [45]. In the present investigation, TOMAWAC has been modified to integrate an additional dissipation term based on van der Westhuysen [46], limiting over-prediction of wave height on negative current gradients.

The numerical resolution is performed on a planar two-dimensional (2D) domain, meshed by means of triangular finite elements. The frequency domain is discretised following a geometric progression, whereas the interval of propagation direction is evenly distributed. The time-dependent spectral action balance equation is solved with a fractional step method, in which the convection and the source-sink term integration steps are solved successively and separately [37, 40]. The propagation step is solved with the method of characteristics, largely employed to process convection equations [47], while the source and sink terms are integrated locally using a semi-implicit scheme. Further details about the mathematical formulations and the numerical schemes are available in the technical documentation [37].

*2.3.2. TELEMAC 3D*

TELEMAC 3D solves the continuity equation and the Reynolds-averaged momentum equations, derived using the Boussinesq approximation and vertical hydrostatic equilibrium. The flow is assumed to be turbulent over a rough bottom, characterised by the roughness parameter $z_0$, defined as the height above the seabed at which the fluid velocity is zero. The horizontal eddy viscosity is parameterised following Smagorinsky [48]. Vertical eddy viscosity is simulated with the mixing length model proposed by Quetin [49], corrected with the damping function introduced by Munk and Anderson [50]. The influence of wind is computed with the coefficient proposed by Flather [51].

Wave-driven currents are simulated using radiation stress theory [12, 52], taking into account the excess flow of momentum due to the presence of waves to calculate the total current. Whereas more complex approaches exist [53], the method used here consists of adding wave-induced forces, considered constant along the vertical, as source terms in the momentum equations [38]. In TOMAWAC, the driving force $\mathbf{F} = (F_x, F_y)$ is thus expressed as follows:

$$F_x = -\frac{1}{d}\left(\frac{\partial S_{xx}}{\partial x} + \frac{\partial S_{xy}}{\partial y}\right), \tag{1}$$

$$F_y = -\frac{1}{d}\left(\frac{\partial S_{yy}}{\partial y} + \frac{\partial S_{yx}}{\partial x}\right) \tag{2}$$

where $d$ is the total water depth and $S_{i,j}$ with $(i, j) \in [x, y]$ are the different components of the radiation stress tensor. The default version of TELEMAC 3D includes only steady-state driving forces. The hydrodynamic model has thus been modified to integrate non-stationary forces in the calculation of wave-driven currents.

A module has also been added to integrate enhancement of bottom friction felt by currents above the wave boundary layer, replacing the roughness parameter $z_0$ by the apparent bottom roughness parameter felt by the current above the wave boundary layer $z_{0b,\omega}$. Wave effects on bottom roughness are computed on the basis of the Signell et al.'s formulation [54], adapted from the original theory of Grant and Madsen [11] on

the interactions between wave and current bottom boundary layers. Assuming a vertical logarithmic velocity profile near the bottom, the apparent bottom roughness parameter is thus expressed as

$$z_{0b,\omega} = \delta_{\omega}^{|1-u_{*c}/u_{*c\omega}|} z_0^{u_{*c}/u_{*c\omega}} \tag{3}$$

where $\delta_\omega = 2\kappa u_{*c\omega}/\omega$ is the thickness of the wave boundary layer, $\kappa$ is von Karman's constant ($\kappa = 0.4$), and $\omega$ is the wave frequency. The total wave and current friction velocity $u_{*c\omega} = \sqrt{\tau_{c\omega}/\rho}$ is computed from the wave and current shear stresses, $\tau_\omega$ and $\tau_c$, as

$$u_{*c\omega} = u_{*\omega}\left[1 + 2\left(\frac{u_{*c}}{u_{*\omega}}\right)^2 |cos\phi_{c\omega}| + \left(\frac{u_{*c}}{u_{*\omega}}\right)^4\right]^{1/4} \tag{4}$$

where $\phi_{c\omega}$ is the angle between wave and current directions, and $u_{*\omega} = \sqrt{\tau_\omega/\rho}$ and $u_{*c} = \sqrt{\tau_c/\rho}$ are the shear velocities arising from the current and the wave, respectively. The shear velocity associated with waves is given by $u_{*\omega} = \sqrt{1/2 f_\omega} U_\omega$, where $f_\omega$ is the wave friction factor evaluated with the empirical relation proposed by Signell et al. [54], and $U_\omega$ is the wave bottom orbital velocity simulated by the wave propagation model. The shear velocity arising from the current alone, $u_{*c}$, is finally computed assuming a vertical logarithmic profile between $z_{0b,\omega}$ and the first vertical grid cell above the bed.

The numerical resolution is performed on a 3D mesh made of prisms generated with a planar 2D domain composed of triangles duplicated along the vertical, following a uniform $\sigma$-transformation. The basic algorithm is split into three fractional steps [55]. The first step solves only the advection terms in the momentum equations. The second step computes, from advected velocities, new velocity components, taking into account diffusion and source terms in the momentum equations. The third and final step computes the total water depth from the depth-averaged continuity and momentum equations. Tidal flats are furthermore considered, applying a correction to free surface gradients, which are equal to the bottom gradient in absence of water and generates spurious terms in the momentum equations [39]. Further details are available in the technical documentation [38].

The theoretical tidal stream energy per unit area (in $\mathrm{W\,m^{-2}}$) is finally calculated by the following expression:

$$P = \frac{1}{2}\rho u^3 \tag{5}$$

where $u$ is the amplitude of the horizontal current component computed by Telemac 3D.

### *2.4. Model setup*

Models were set up on unstructured computational grids covering the western extent of Brittany, and comprising 6929 nodes for TOMAWAC and 8293 nodes for TELEMAC 3D (Fig. 3). The size of triangular elements extends from 10 km at the offshore boundaries to less than 50 m in the Fromveur Strait. Whereas increased spatial resolutions may be achieved in the area of interest to refine the approach of quantifying the available tidal stream power, particularly contributions of sub-regional eddies [56], the computational mesh retained here offers an attractive compromise between resolving the major influence of waves on tidal currents and non-prohibitive CPU resources. The bathymetry is derived from a compilation of different databases, including (1) offshore: the large-scale database

of Loubrieu [57] covering the English Channel and the Bay of Biscay with a spatial resolution of 1 km, (2) the Sea of Iroise: bathymetric surveys provided by the French Navy SHOM and (3) the Molène-Ushant archipelago: the high-resolution coverage established during the Litto3D project [58].

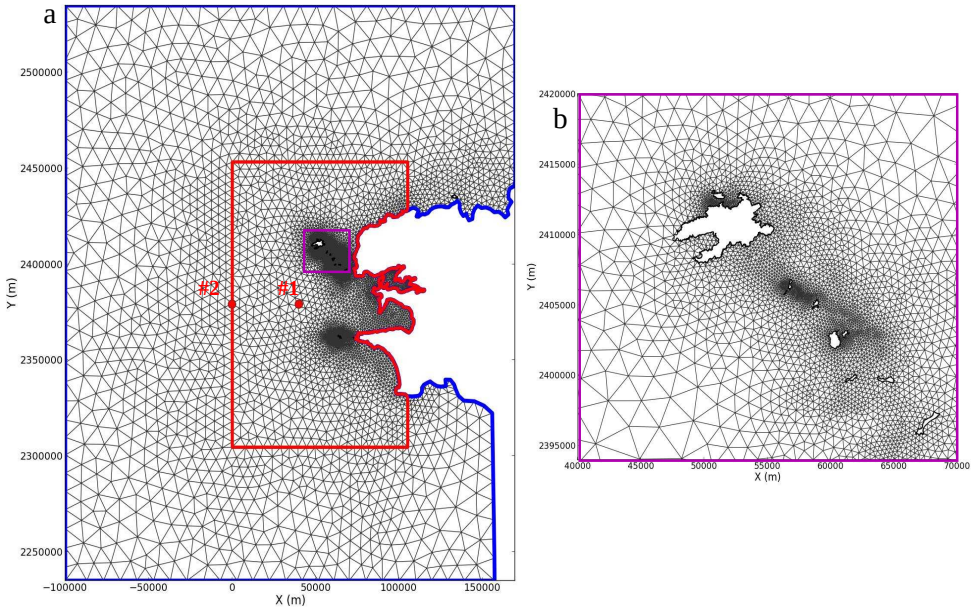


Figure 3: (a) Computational grids for (blue line) TELEMAC 3D and (red line) TOMAWAC with locations of points #1 and #2. (b) Detailed view of the unstructured computational grid in and around the Fromveur Strait.

TOMAWAC was configured with 31 exponentially spaced frequencies, ranging from 0.05 to 1 Hz, 15 evenly spaced directions, and a time step of 20 s. Hourly wind velocity components at 10 m above the free surface are provided at 0.2 ° spatial resolution by the Climate Forecast System Reanalysis Version 2 (CFSRv2) [59]. The wave model integrates variations of free-surface elevation and depth-averaged currents predicted by TELEMAC 3D every 15 min. TOMAWAC is driven by JONSWAP wave spectra established on the basis of integrated parameters of significant wave height, peak period, direction and spreading. These parameters are predicted along open boundaries of the TOMAWAC computational domain by a regional run of WaveWatch III (WWIII) over the north-eastern Atlantic ocean, at three hourly intervals with a spatial resolution of 18 km, in the context of the IOWAGA project (Integrated Ocean WAves for Geophysical and other Applications, Ifremer, France) [60].

TELEMAC 3D is implemented with $11 - \sigma$ vertical-grid cells following previous numerical investigations of tidal flow in the Sea of Iroise [18, 61], and a time step of 20 s. The bottom roughness associated with the sea bed is determined, from the offshore extent of the isle of Ushant to the eastern boundary, on the basis of the map established by Hamdi et al. [62] (Ifremer, "Agence des Aires Marines Protégées") and observations for different bottom types compiled by Soulsby [63]. The offshore bottom roughness is set

to a uniform value of $k_n = 10.5$ mm. Wind velocity components derive also from CFSv2 at an hourly time step. Wave data are imposed at hourly intervals at the scale of the TOMAWAC computational domain (Fig. 3), while zero values are considered outside. The 3D hydrodynamic model is finally driven by 13 major harmonic tidal constituents ($K_1$, $O_1$, $P_1$, $Q_1$, $M_2$, $S_2$, $N_2$, $K_2$, $M_4$, $MS_4$, $MN_4$, $M_m$, $M_f$) derived from the TPXO7.2 database [64], which has a spatial resolution of 0.25 °.

The modelling system was run during two periods: (1) November 2012 for assessment of TOMAWAC model performance and (2) March-April 1993 for evaluation of the TELEMAC 3D predictions. Effects of waves on tidal stream power are evaluated with four numerical experiments entitled A to D (Table 3). Experiment A neglects wave effects. Experiments B and C integrate the influences of wave forces and enhanced bottom friction, respectively. Experiment D incorporates combined effects. Numerical results of the effects of waves on tidal currents are thus evaluated during the second period with the standard statistical parameters of the mean absolute and relative differences, $\mathrm{DIFF}_{\mathrm{abs}} = \frac{1}{n}\sum_{i=1}^{i=n}|y_i - x_i|$ and $\mathrm{DIFF}_{\mathrm{rel}} = \frac{1}{n}\sum_{i=1}^{i=n}(y_i - x_i)$, the index of agreement RE [65], and the Pearson's correlation coefficient R where $n$ is the number of data in the discretised series considered, $(x_i)$ and $(y_i)$ represent the two sets of observed and simulated data, respectively.

Table 3: List of numerical experiments retained for the evaluation of effects of waves on tidal stream power.

| Numerical experiments | Waves forces | Waves enhanced bottom friction |
|---|---|---|
| A | | |
| B | ✓ | |
| C | | ✓ |
| D | ✓ | ✓ |

## 3. Results and discussion

### *3.1. Evaluation of model predictions*

#### *3.1.1. Waves*

The evaluation of wave model predictions is performed against in-situ measurements of significant wave height $H_s$, peak wave period $T_p$, and mean wave directions at the two wave buoys throughout November 2012 (Fig. 4). Whereas waves experience significant inter-annual variability in the area of interest [15, 42], the mean distribution of wave events at the shallow wave buoy established from predictions over a eight-year period [16] (Fig. 5) demonstrates that the observed data are representative of a wide range of waves conditions at the measurement location. Generally, $H_s$ was in the range 1-2 m, while a storm event on 23 November led to values of significant wave height in excess of 3 m. Model simulations at the two wave buoys reproduced the temporal evolution of observed parameters, with statistical evaluations of $H_s$ and $T_p$ in agreement with estimations reported by Boudière et al. [66] at the deep water wave buoy (Table 4). Good agreement

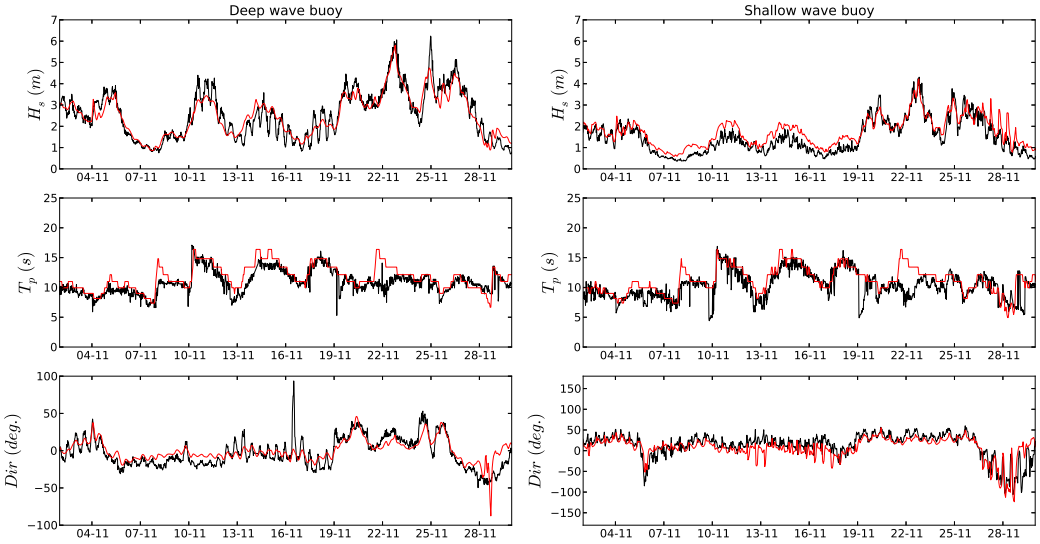


Figure 4: Measured (black line) and TOMAWAC computed (red line) time series of significant wave height, peak period and mean wave direction (anticlockwise convention from the East) at wave buoys in November 2012.

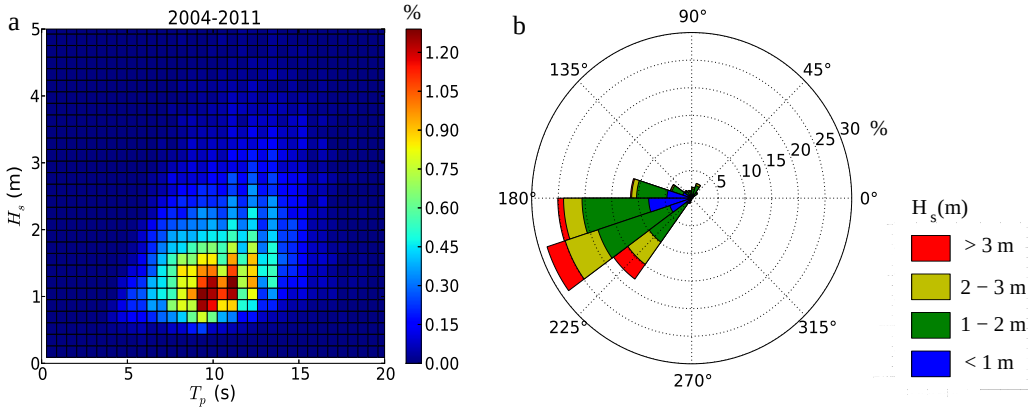


Figure 5: (a) Distribution of wave events, established from predictions for the period 2004-2011 [16], shown as significant wave height against peak wave period at the shallow wave buoy. (b) Associated direction distribution.

is thus obtained, at this point, for the significant wave height, with indexes RE and R of 0.96 and 0.94, respectively. Increased differences between model and observations are however obtained in peak period estimations. Nevertheless, indexes of agreement RE remain over 0.81 at both measurement locations, indicating no particular bias in wave predictions. Whereas numerical results at the deep water wave buoy under-estimated semi-diurnal modulations induced by tidal currents, the agreement between simulations and measurements improves at the shallow water wave buoy, due to a reduction of tidal

modulation in the Fromveur Strait.

Table 4: Summary statistics for significant wave height $H_s$ and peak period $T_p$ at deep and shallow water wave buoys in November 2012.

| Wave | $H_s$ | | | $T_p$ | | |
|---|---|---|---|---|---|---|
| buoys | $\text{DIFF}_{\text{abs}}$ (m) | RE | R | $\text{DIFF}_{\text{abs}}$ (s) | RE | R |
| Deep wave buoy | 0.30 | 0.96 | 0.94 | 1.13 | 0.84 | 0.78 |
| Shallow wave buoy | 0.34 | 0.92 | 0.92 | 1.37 | 0.81 | 0.70 |

Wave model performance was further assessed over the period of current measurements, by comparing predictions with WWIII numerical results, issued from the IOWAGA project [60], at point #1 ($\lambda = 5.20$ ° W, $\phi = 48.17$ ° N) located off the Ushant-Molène archipelago (Figs. 3 and 6). WWIII was set up at the scale of the north-eastern Atlantic ocean on a computational grid with a spatial resolution between 0.2 and 0.25 °. Whereas this simulation integrates wind forcings from the CFSR reanalysis and variations of free-surface elevations and depth-averaged currents [66], parameterisations retained for wind wave generation and dissipation [67] show major differences with the modelling setup of TOMAWAC in the present investigation. Nevertheless, WWIII simulations have been thoroughly assessed against a series of in-situ observations and altimeter data in the area of interest [66, 67], promoting the use of these simulations for further evaluation of TOMAWAC results over the period of current measurements. Good agreement was obtained between TOMAWAC and WWIII simulations, despite some discrepancy in the mean wave direction around the 27 March. TOMAWAC predictions are thus considered sufficiently accurate for the evaluation of wave-induced variations of the available tidal stream power in the Fromveur Strait.

*3.1.2. Tidal stream power*

Attention will be devoted to effects at 10 m above the bed as this corresponds to the operating height of horizontal axis turbines such as Sabella D10 in the Strait. Predictions from the 3D circulation model in the absence of waves (experiment A) are assessed against in-situ observations of tidal stream power and current direction 10 m above the bed at the ADCP site during March 1993 (Fig. 7). This vertical level is representative of tidal kinetic energy extraction from the Sabella D10 device in the Fromveur Strait (Section 2.1).

An overall good agreement is obtained between measurements and predictions of tidal stream power. Whereas simulations over-estimate south-west directed current observations by $10 - 15$ % during storm events (24-25 March), numerical results reproduce well the spring-neap tidal modulations of observed tidal stream power. Despite a slight deviation, simulated current direction is consistent with in-situ measurements, reproducing abrupt changes between south-west and north-east directed velocities.

*3.2. The effect of waves on tidal kinetic energy*

*3.2.1. Local effects*

Fig. 8 presents statistical parameters for predictions of tidal stream power 10 m above the bed for configurations A to D between 20 March, 00:00 UTC and 30 March 1993,

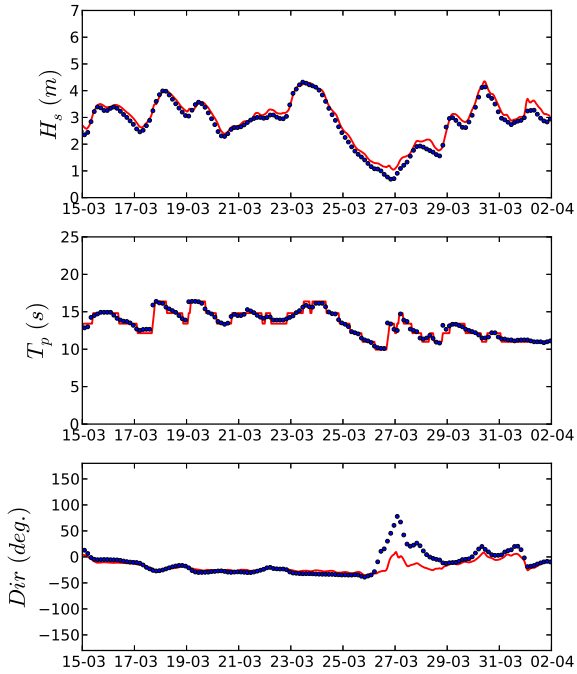


Figure 6: Time series of significant wave height, peak period, and mean wave direction computed from TOMAWAC (red line) and WW3 (blue points) at point #1 in March-April 1993.

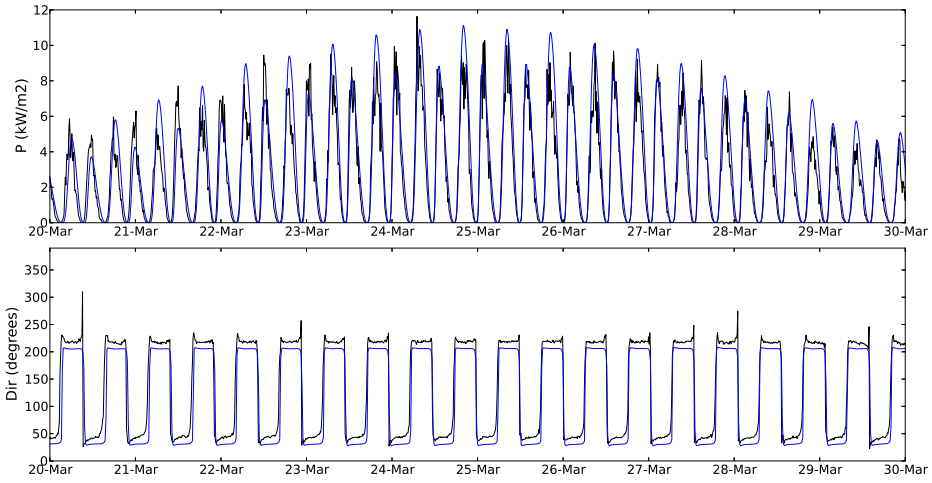


Figure 7: Measured (black line) and computed time series of tidal stream power and current direction in the absence of waves (experiment A, blue line) 10 m above the bed at the ADCP site in March 1993. Direction is displayed with an anticlockwise convention from the East. A direction of 210 $^{o}$ corresponds to south-west directed currents, while a direction of 30 $^{o}$ corresponds to north-eastern directed currents.

00:00 UTC (Fig. 7). The inclusion of waves appears to improve numerical simulations for the three configurations B (waves forces), C (enhanced bottom friction) and D (combined effects). Whereas reduced differences are obtained with the integration of waves forces (B), more significant effects appear under the influence of increased apparent bottom roughness (C and D). The relative averaged difference in the reference configuration A decreases from 3.5 % with wave-driven currents (experiment B), while it is reduced by 17.5 % when interactions between wave and current bottom boundary layers (experiment C) are included (Fig. 8-a). The combination of waves forces and enhanced bottom friction (experiment D) results in the best estimate of tidal stream power, with an index of agreement of 0.96 for the period of comparison (Fig. 8-b).

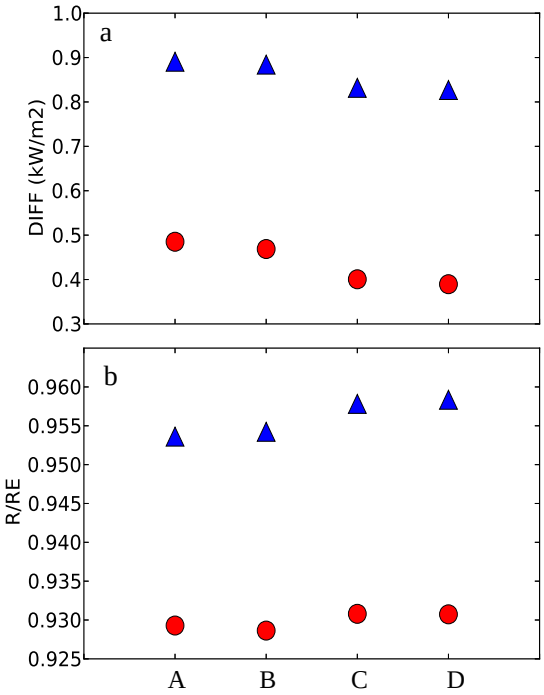


Figure 8: (a) Absolute (blue) and relative (red) differences, $\mathrm{DIFF}_{\mathrm{abs}}$ and $\mathrm{DIFF}_{\mathrm{rel}}$, between measurements and predictions of tidal stream power 10 m above the bed at the ADCP site, between 20 March, 00:00 UTC and 30 March 1993, 00:00 UTC, for the four configurations A-D. (b) Associated index of agreement RE (blue) and Pearson's correlation coefficient R (red).

Fig. 9 shows the temporal evolution at the ADCP site of differences in predicted tidal stream power for configurations B, C and D with respect to the reference configuration A. Wave-induced variations prevail during storm conditions of 24 and 30 March 1993 (Fig. 6). These effects are exhibited during times of peak tidal current amplitudes, leading to quarter-diurnal variations of wave-induced modulations. The combined influence of wave forces and enhanced bottom friction (experiment D) results in a maximum reduction of tidal stream power of 1.0 $\mathrm{kW\,m^{-2}}$ on 24 March 1993. This 9 % reduction of total kinetic energy is consistent with reductions reported by Hashemi et al. [29] of around 15 % for mean wave scenarios off the north-west coast of Anglesey (UK).

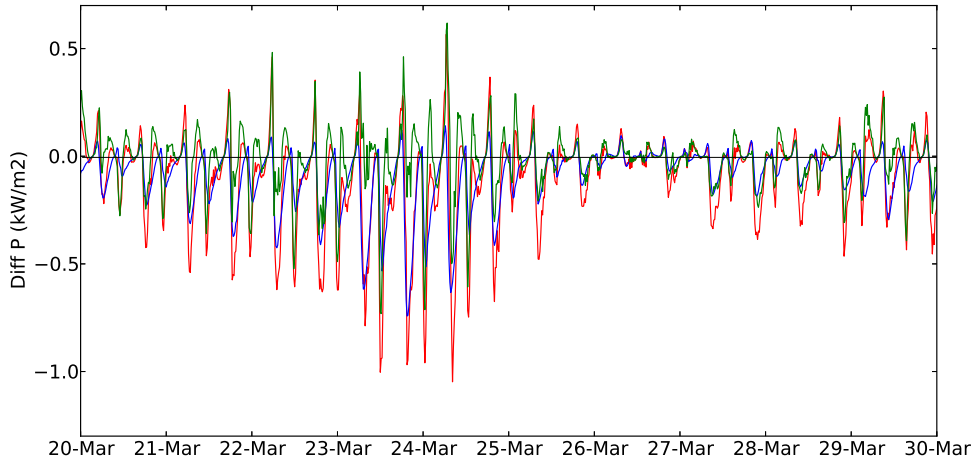


Figure 9: Time series of differences in predicted tidal stream power 10 m above the bed at the ADCP site with respect to the reference configuration A (without waves) for configurations B (green, waves forces), C (blue, enhanced bottom friction) and D (red, combined effects). Negative values indicate a reduction in kinetic energy.

Inclusion of wave forces has less influence on tidal stream power than enhanced bottom friction at the measurement point (Fig. 8). The peak tidal stream power of 24 March 1993 is reduced by 0.49 $\mathrm{kW\,m^{-2}}$ with wave-driven currents (experiment B), while it is reduced by 0.59 $\mathrm{kW\,m^{-2}}$ with enhanced bottom friction (experiment C) (Fig. 9). This corresponds to an instantaneous reduction in kinetic energy of 4.4 and 5.3 %, respectively. The inclusion of wave forces, however, contributes to a slight increase in tidal stream power at times of slack water (Fig. 9), mainly because associated wave-driven currents modify the hydrodynamic flow field with noticeable effects during times of reduced tidal flow. Further, enhanced bottom friction appears to result in a more pronounced reduction of tidal stream power for south-west directed currents. This evolution is mainly attributed to the modulation of $u_{*c\omega}$ (Eq. 4) by the angle between wave and current direction. At the measurement point, $|\cos\phi_{c\omega}|$ is increased for south-west directed currents, in comparison with north-east directed currents. The total wave and current friction velocity is thus increased, resulting in enhanced bottom friction and a reduction in near-bottom currents during this period. This process leads to a reduction in the over-estimate of south-west directed current amplitude, as exhibited in Fig. 10, improving numerical estimates of tidal stream power at 10 m above the seabed.

*3.2.2. Synoptic effects*

The spatial distribution of averaged simulated tidal stream power during spring-neap tidal conditions of March 1993 (from 16 March, 16:55 UTC to 31 March, 15:35 UTC) (Fig. 11-a) appears consistent with estimates made by Thiébaut and Sentchev [33] in the Fromveur Strait. Over the area identified for array implementation, mean kinetic energy during spring-neap tidal conditions falls within the range $2-3$ $\mathrm{kW\,m^{-2}}$, with noticeably strong values (over 4 $\mathrm{kW\,m^{-2}}$) in the south-eastern part of this area. Whereas enhanced bottom friction results in a global decrease of tidal stream power (Fig. 11-c), wave forces

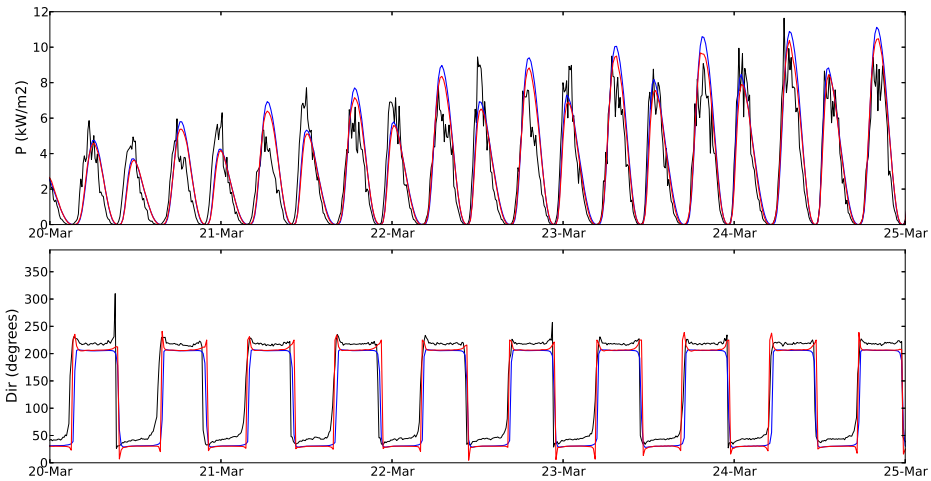


Figure 10: Measured (black line) and computed time series of tidal stream power and current direction (anticlockwise convention from the East) without (experiment A, blue line) and with (experiment D, red line) waves 10 m above the bed at the ADCP site in March 1993.

are found to increase kinetic energy (1) in the nearshore exposed areas of the isle of Ushant, and (2) along the south-eastern part of the Strait (Fig. 11-b). Such localised increases in tidal stream power have also been reported by Hashemi et al. [29]; the presence of wave forces leading to new hydrodynamic current field in regions where there are strong gradients of wave radiation stresses. However, the combined effects of wave forces and enhanced bottom friction result in a reduction of available kinetic energy at the scale of the area identified for tidal stream array implementation, particularly noticeable in the north-west of the region (Fig. 11-d). Tidal stream power is thus found to decrease by 4 % in the north-western part of the Strait, while reduced tidal stream power, restricted to 1 %, is obtained in the south-eastern part of the Strait. Whereas these differences may appear negligible with respect to uncertainty in model predictions in the area of interest, they do demonstrate a slight tendency of waves to an increase in the spatial gradient of mean available kinetic energy identified across the main flow in the Fromveur Strait (Fig. 11).

### *3.3. Analysis for stationary offshore wave conditions*

#### *3.3.1. Scenarios selected*

Further analysis of the model simulations was conducted, based on mean and extreme wave conditions in the Sea of Iroise. Based on wave statistics at point #2 ($\lambda = 5.74$ ° W, $\phi = 48.13$ ° N) located at the western offshore boundary of the TOMAWAC computational domain (Figs. 3 and 12), two scenarios, entitled W1 and W2, were selected(Table 5). These configurations correspond to mean and extreme wave conditions at point #2. Simulations were performed for mean spring tidal conditions, resulting in averaged and maximum tidal stream powers of 8 and 21 kW m$^{-2}$, respectively, in the south-eastern part of the Strait (Fig. 13). A mean south-westerly wind speed of 7.5 m s$^{-1}$ was obtained from the analysis of wind climatology in the region of interest. Whereas offshore stationary

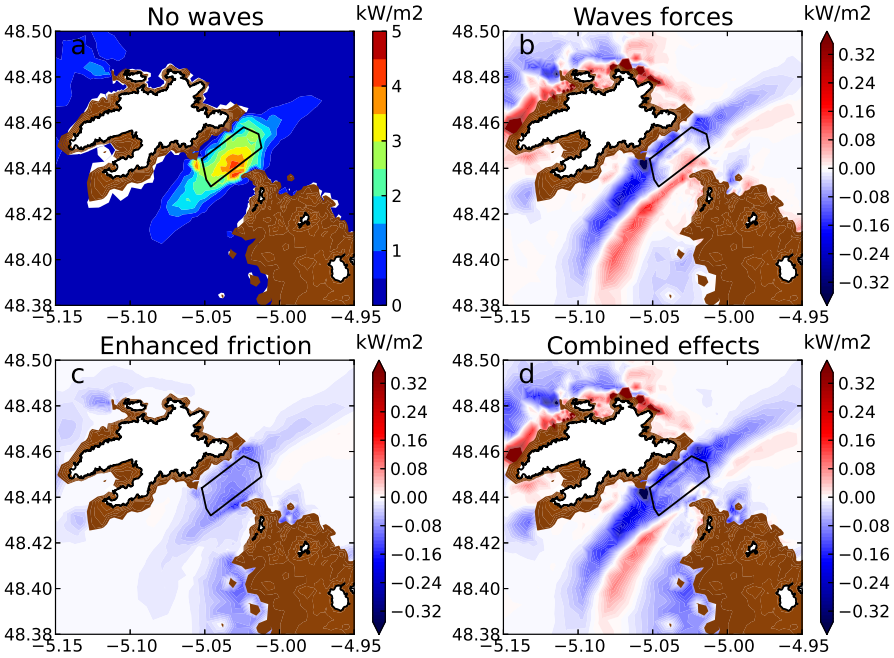


Figure 11: (a) Averaged predicted tidal stream power 10 m above the bed during a neap-spring tidal cycle of March 1993 (from 16 March, 16:55 UTC to 31 March, 15:35 UTC) for the reference configuration A without waves. Relative differences with respect to these reference predictions are shown for configurations with (b) waves forces, (c) enhanced bottom friction, and (d) combined effects. Predictions are shown for mean water depths over 20 m. Positives values indicate an increase of mean tidal stream power, while negative values indicate reduced kinetic energy.

wave conditions are considered at the boundary for configurations W1 and W2, waves evolve within the computational domain, under the effects of tidal free-surface elevation and currents.

Table 5: Scenarios selected for the analysis in stationary offshore wave conditions. The incoming wave direction is displayed with an anticlockwise convention convention from the East.

| Configuration | $H_s$ (m) | $T_p$ (s) | Dir. ( $^o$) |
|---|---|---|---|
| W1 | 2.6 | 11.0 | 171 |
| W2 | 5.0 | 14.0 | 171 |

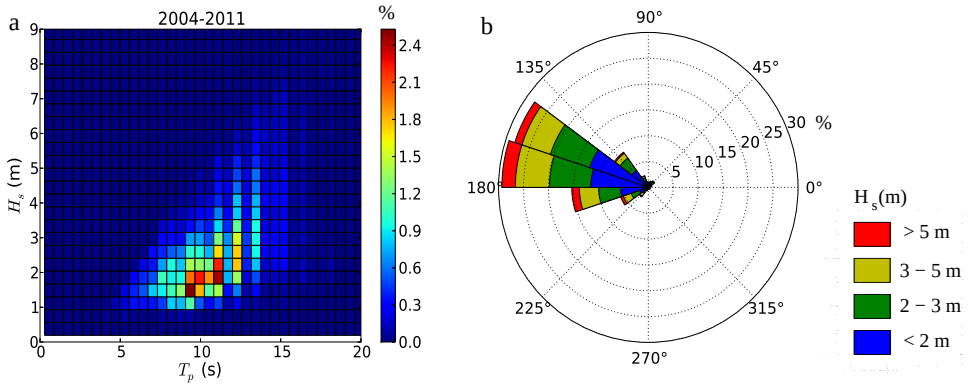


Figure 12: (a) Distribution of wave events, established from predictions for the period 2004-2011 [16], shown as significant wave height against peak wave period at the western offshore boundary of the computational domain (point #2). (b) Associated direction distribution.

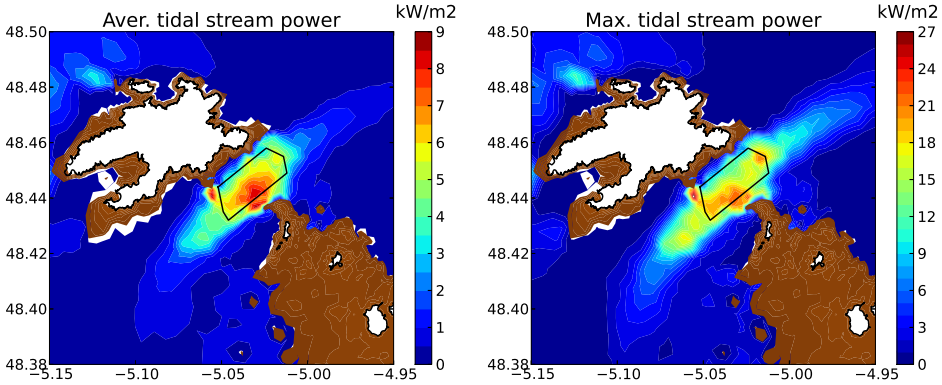


Figure 13: Averaged and maximum predicted tidal stream power 10 m above the bed during mean spring tidal conditions, neglecting wave effects.

### *3.3.2. Detailed analysis*

Fig. 14 shows differences in averaged predicted tidal stream power 10 m above the seabed during mean spring conditions for configuration W1. The evolution of tidal stream potential presents globally similar patterns to those identified previously (Fig. 11), confirming simulations established during neap-spring conditions of March 1993. In order to gain further insights regarding spatial differences obtained for wave forces and enhanced bottom friction in Figs. 11 and 14, a refined analysis of model outputs was conducted at times of peak flood and ebb currents in the Strait (Figs. 15 and 16).

Wave forces are found to increase kinetic energy 10 m above the seabed along the south-eastern part of the Strait, while reducing tidal stream power in the north-western region (Fig. 14-a). These differences are more specifically identified at time of peak ebb currents in the Strait (Fig. 15). During this period, wave-driven currents are found

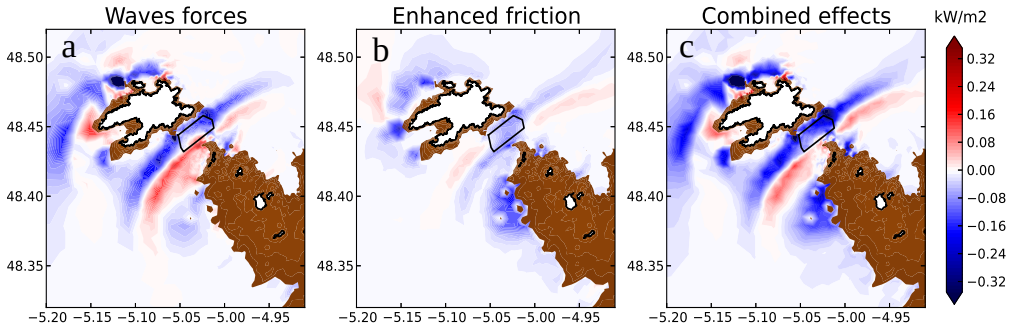


Figure 14: Differences in averaged predicted tidal stream power 10 m above the bed during mean spring conditions for configuration W1 with (a) waves forces, (b) enhanced bottom friction, and (c) combined effects.

to increase currents in the shallow waters around shoals and islands. This results, in particular, in a stronger amplitude of depth-averaged currents on both sides of the ebb stream passing the Fromveur Strait. Current amplitude is, however, reduced in the ebb stream. Whereas further observations are required, possible compensation effects, by the model, of the flow passing the Strait may explain this spatial distribution.

While enhanced bottom friction leads to a reduction in kinetic energy in the area of interest, synoptic differences reveal slight increases in tidal stream power $\sim 0.04\ \mathrm{kW\,m^{-2}}$ at the south-western and north-eastern limits of the Strait (Fig. 14-b). Synoptic representations of depth-averaged currents during flood and ebb peaks (Fig. 16) exhibit a significant reduction of around $15 - 20\ \%$ of current amplitude in nearshore areas and shoals surrounding the isle of Molène. Such effects are consistent with estimations performed by Guillou and Chapalain [13] in the southern Dover Strait during storm conditions. Reduction of current amplitude is, however, restricted to $2\ \%$ in the deeper waters of the Fromveur Strait. In the Strait, the current amplitude is reduced in exposed areas where the tidal currents act in the same direction as wave propagation, amplifying combined wave and current shear stress (Eq. 4) and the associated apparent bottom roughness (Eq. 3). These areas correspond to the north-western part of the Strait during flood, and the south-eastern part during ebb (Fig. 16). As noted for the influence of wave forces, compensation effects of the flow through the Strait may explain the slight increase in stream power obtained in Fig. 14.

*3.3.3. Evolution of tidal stream power*

Although wave forces are found to slightly increase tidal stream power by $1 - 2\ \%$ in the south-eastern part of the area that has been identified for array implementation, the global tendency is a reduction of kinetic energy 10 m above the bed. Over the planned tidal stream array, the averaged value of predicted mean tidal kinetic power during mean spring conditions is thus reduced, under combined wave effects (experiment D), by $2.0\ \%$ and $12\ \%$ for mean and extreme wave conditions, respectively (Fig. 17). This reduction may reach $15.2\ \%$ of the averaged value of maximum tidal stream power over the area identified for array implementation, for extreme wave conditions (configuration W2) and combined waves effects (experiment D). These estimates are consistent with Hashemi

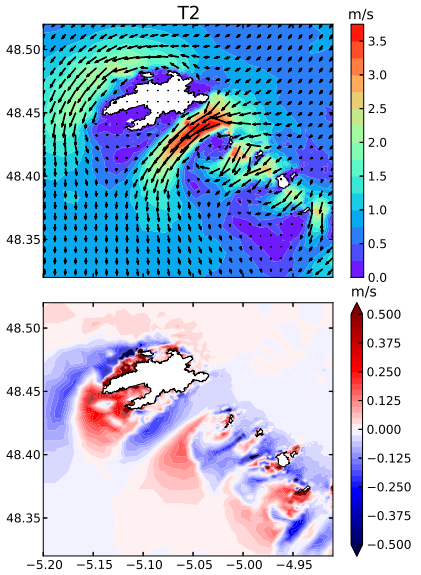


Figure 15: (Top) Depth-averaged currents without waves and (bottom) differences in the amplitude of depth-averaged currents by integrating the effects of waves forces in configuration W1 at time of ebb peak (T2) at the ADCP site, during mean spring conditions. Positive and negative values account for increase and reduction of currents, respectively.

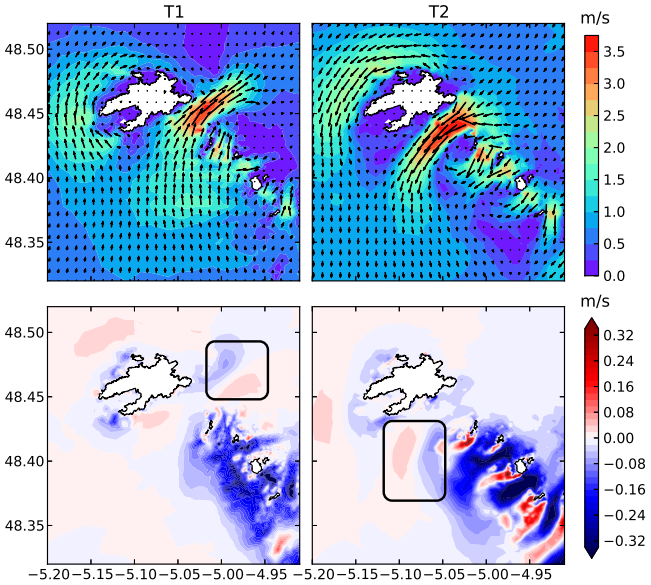


Figure 16: (Top) Depth-averaged currents without waves and (bottom) differences in the amplitude of depth-averaged currents by integrating the effects of enhanced bottom friction in configuration W1 at times of flood (T1) and ebb (T2) peaks at the ADCP site, during mean spring conditions.

et al. [29], who reported a reduction of up to 15 % and 20 % for mean and extreme winter wave scenarios, respectively, at the Skerries tidal stream site in the Irish Sea. Whereas local comparison at the ADCP site shows stronger effects of enhanced bottom friction than wave forces (Fig. 8), the global assessment at the scale of the region of interest exhibits more significant reduction due to wave-driven currents. During extreme wave conditions (configuration W2), the mean kinetic energy over the planned stream array is thus reduced by 7.8 % with wave forces, compared to a reduction of 5.3 % with enhanced bottom friction. These differences correspond to 11.2 and 6.5 % of the maximum available tidal stream potential. This is mainly attributed to a more significant attenuation of kinetic energy by inclusion of wave forces in the north-western part of the region of interest (Fig. 14-a).

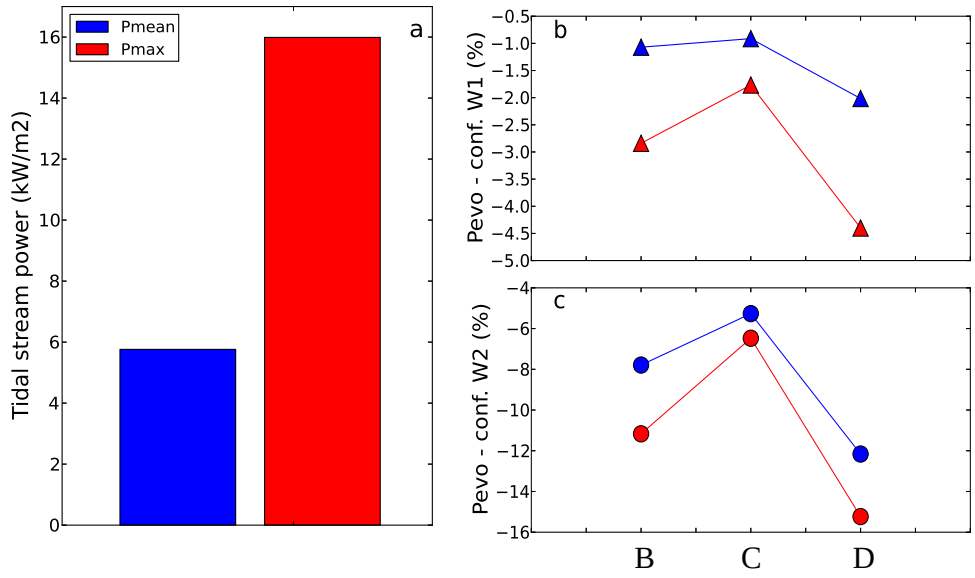


Figure 17: (a) Predicted mean and maximum tidal stream power averaged over the area identified for array implementation during mean spring conditions without waves (configuration A). Evolution of averaged (blue) mean and (red) maximum tidal stream power for configurations B (wave forces), C (enhanced friction) and D (combined effects) and wave conditions derived from cases (b) W1 and (c) W2.

## 4. Conclusions

The 3D tidal circulation model TELEMAC 3D, coupled with the wave propagation model TOMAWAC, has been applied to a region off western Brittany to investigate and evaluate effects of (1) wave-induced forces and (2) enhanced bottom friction resulting from wave-current interaction in the bottom boundary layer on available tidal kinetic energy in the Fromveur Strait. Numerical results have been compared with a series of in-situ measurements of significant wave height, peak wave period, mean wave direction, along with data on current amplitude and direction at 10 m above the seabed. The main outcomes of the present study are as follows.

1. Inclusion of wave effects in the 3D tidal model improves simulations of tidal stream power 10 m above the seabed, and reduces peak kinetic energy by up to 9 % at the measurement site during storm conditions.
2. Waves appear to increase the spatial gradient of available mean stream power across the Fromveur Strait, resulting in a slightly stronger reduction of kinetic energy in the north-western region than in the south-eastern region of the Strait.
3. Wave radiation stresses were found to increase kinetic energy along the south-eastern part of the Strait, while concurrently reducing tidal stream power in the north-western part of the Strait. Despite a slight increase in simulated tidal stream power, enhanced bottom friction acts to reduce kinetic energy in the Strait. At the scale of the planned tidal stream array, extreme wave conditions lead to a reduction of maximum available spring tidal stream potential by 11.2 and 6.5 % for wave forces and enhanced bottom friction, respectively. Combined effects lead to a reduction of tidal stream power by 15.2 %.

Whereas further investigations may be required to assess 3D model predictions in comparison with depth-averaged simulations, improvements of numerical results may also be reached with (1) refined approaches of current-induced modulations of waves in the Strait and (2) better definition of bottom friction. Nevertheless, the present investigation provides interesting insights into the effects of waves on the available kinetic energy within the Fromveur Strait; of noticeable interest for potential developers of tidal energy converters in this region. Refined quantification of wave effects would benefit from extended concurrent measurements of waves and tidal currents in the Strait, in particular in areas where a decrease/increase of stream power was identified by the present numerical modelling work. Over a longer time period, improved numerical modelling could be used to help analyse the inter-annual and inter-seasonal variabilities of tidal kinetic energy induced by waves in the Fromveur Strait.

## Acknowledgements

Wave data used at open boundaries of the wave propagation model were obtained from regional runs of WaveWatch III within the context of the IOWAGA project (http://wwz.ifremer.fr/iowaga/Products). Current measurements were supplied by the Service Hydrographique et Océanographique de la Marine (SHOM), and wave buoy data was provided by the French CANDHIS database (Cerema). The authors are furthermore grateful to André Simon (Cerema) for the process of sedimentological data. Simulations were performed on computer facilities CAPARMOR (CAlcul PARallèle Mutualisé pour l'Océanographie et la Recherche). The present paper is a contribution to the research programs DIADEMS and FLUSED of the Laboratory of Coastal Engineering and Environment (Cerema, http://www.cerema.fr, http://memphys-lgce.fr.ht). S. P. Neill wishes to acknowledge the support of the Sêr Cymru National Research Network for Low Carbon, Energy and the Environment (NRN-LCEE).

## References

[1] J. Goundar, M. R. Ahmed, Design of a horizontal axis tidal current turbine, Applied Energy 111 (2013) 161–174.

[2] D. Magagna, A. Uihlein, Ocean energy development in Europe: Current status and future perspectives, International Journal of Marine Energy 11 (2015) 84–104.
[3] P. Robins, S. Neill, M. Lewis, S. Ward, Characterising the spatial and temporal variability of the tidal-stream energy resource over the northwest European shelf seas., Applied Energy 147 (2015) 510–522.
[4] E. Kirinus, W. Marques, Viability of the application of marine current power generators in the south brazilian shelf, Applied Energy 155 (2015) 23–34.
[5] P. Work, K. Haas, Z. Defne, T. Gay, Tidal stream energy site assessment via three-dimensional model and measurements, Applied Energy 102 (2003) 510–519.
[6] M. Sánchez, R. Carballo, V. Ramos, G. Iglesias, Tidal stream energy impact on the transient and residual flow in an estuary: A 3D analysis, Applied Energy 116 (2014) 167–177.
[7] S. Neill, M. Hashemi, M. Lewis, The role of tidal asymmetry in characterizing the tidal energy resource of Orkney, Renewable Energy 68 (2014) 337–350.
[8] D. Coles, L. Blunden, A. Bahaj, Energy extraction potential from the Alderney Race, in: 11th European Wave and Tidal Energy Conference, Nantes, France, 2015, pp. 08D4–1–1–9.
[9] L. Myers, A. Bahaj, Simulated electrical power potential harnessed by marine current turbine arrays in the Alderney Race, Renewable Energy 30 (2005) 1713–1731.
[10] M. Olabarrieta, R. Medina, S. Castanedo, Effects of wave-current interaction on the current profile, Coastal Engineering 57 (2010) 643–655.
[11] W. Grant, O. Madsen, Combined wave and current interaction with a rough bottom, Journal of Geophysical Research 84 (C4) (1979) 1797–1808.
[12] M. Longuet-Higgins, R. Stewart, Radiation stresses in water waves; a physical discussion, with applications, Deep-Sea Research 11 (1964) 529–562.
[13] N. Guillou, G. Chapalain, Modelling impact of northerly wind-generated waves on sediments resuspensions in the Dover Strait and adjacent waters, Continental Shelf Research 31 (2011) 1894–1903.
[14] P. Bonneton, J. Lefebvre, P. Bretel, S. Ouillon, P. Douillet, Tidal modulation of wave-setup and wave-induced currents on the Aboré coral reef, Journal of Coastal Research 50 (2007) 762–766.
[15] S. Neill, M. Hashemi, Wave power variability over the northwest European shelf seas, Applied Energy 106 (2013) 31–46.
[16] N. Guillou, G. Chapalain, Numerical modelling of nearshore wave energy resource in the Sea of Iroise, Renewable Energy 83 (2015) 942–953.
[17] N. Guillou, G. Chapalain, Wave energy potential in the Sea of Iroise, in: 11th European Wave and Tidal Energy Conference Series, Nantes, France, 2015.
[18] N. Guillou, G. Chapalain, E. Duvieilbourg, Modelling impact of bottom roughness on sea surface temperature in the Sea of Iroise, Continental Shelf Research 54 (2013) 80–92.
[19] L. Jia, Y. Wen, S. Pan, J. Liu, J. He, Wave-current interaction in a river and wave dominant estuary: A seasonal contrast, Applied Ocean Research 52 (2015) 151–166.
[20] Z. Rong, R. Hetland, W. Zhang, X. Zhang, Current-wave interaction in the Mississippi-Atchafalaya river plume on the Texas-Louisiana shelf, Ocean Modelling 84 (2014) 67–83.
[21] E. Lust, L. Luznik, K. Flack, J. Walker, M. V. Benthem, The influence of surface gravity waves on marine current turbine performance, International Journal of Marine Energy 3-4 (2013) 27–40.
[22] L. Luznik, K. Flack, E. Lust, K. Taylor, The effect of surface waves on the performance characteristics of a model tidal turbine., Renewable Energy 58 (2013) 108–114.
[23] T. Jesus Henriques, S. Tedds, A. Botsari, G. Najafian, T. Hedges, C. Sutcliffe, I. Owen, R. Poole, The effects of wave-current interaction on the performance of a model horizontal axis tidal turbine, International Journal of Marine Energy 8 (2014) 17–35.
[24] S. Tatum, C. Frost, M. Allmark, D. O'Doherty, A. Mason-Jones, P. Prickett, R. Grosvenor, C. Byrne, T. O'Doherty, Wave-current interaction effects on tidal stream turbine performance and loading characteristics, International Journal of Marine Energy 14 (2016) 161–179.
[25] M. Hashemi, S. Neill, The role of tides in shelf-scale simulations of the wave energy resource., Renewable Energy 69 (2014) 300–310.
[26] A. Saruwatari, D. Ingram, L. Cradden, Wave-current interaction effects on marine energy converters, Ocean Engineering 73 (2013) 106–118.
[27] M. Hashemi, S. Grilli, S. Neill, A simplified method to estimate tidal current effects on the ocean wave power resource, Renewable Energy 96 (2016) 257–269.
[28] M. Lewis, S. Neill, M. Hashemi, M. Reza, Realistic wave conditions and their influence on quantifying the tidal stream energy resource, Applied Energy 136 (2014) 495–508.
[29] M. Hashemi, S. Neill, P. Robins, A. Davies, M. Lewis, Effect of waves on the tidal energy resource at a planned tidal stream array., Renewable Energy 75 (2015) 626–639.

[30] E. Wolanski, J. Imberger, M. Heron, Island wakes in shallow coastal waters, Journal of Geophysical Research 89 (1984) 10553–10569.
[31] F. Hinschberger, A. Guilcher, M. Pruleau, A. Moign, Y. Moign, Carte sédimentologique sous-marine des côtes de France. Feuille de Brest. Echelle 1/100000., Tech. rep., DGRST-CNEXO (1968).
[32] SHOM, Courants de marée - Côte Ouest de Bretagne, Technical Report, Service Hydrographique et Océanographique de la Marine (1994).
[33] M. Thiébaut, A. Sentchev, Estimation of tidal stream potential in the Iroise Sea from velocity observations by high frequency radars, Energy Procedia 76 (2015) 17 – 26, European Geosciences Union General Assembly 2015 - Division Energy, Resources and Environment, EGU 2015.
[34] F. Ardhuin, A. Roland, F. Dumas, A.-C. Bennis, A. Sentchev, P. Forget, J. Wolf, F. Girard, P. Osuna, M. Benoit, Numerical wave modeling in conditions with strong currents: dissipation, refraction, and relative wind, Journal of Physical Oceanography 42 (2012) 2101–2120.
[35] Sabella, Baptême de l'hydrolienne Sabella D10, dossier de presse, Tech. rep., Sabella (2015).
[36] J. C. Allo, Marine current energy for islands, in: Proceedings of IRENA - Martinique conference on island energy transitions, Martinique, 2015.
[37] EDF R&D, TOMAWAC - Software for sea state modelling on unstructured grids over oceans and coastal seas, Tech. rep., EDF (2011).
[38] EDF R&D, TELEMAC modelling system - TELEMAC-3D software - release 6.2, Tech. rep., EDF (2013).
[39] J. Hervouet, Hydrodynamics of free surface flows, modelling with the finite element method, Cambridge University Press, Cambridge, 2007.
[40] M. Benoit, F. Marcos, F. Becq, Development of a third generation shallow-water wave model with unstructured spatial meshing, in: Proceedings of the 25th International Conference on Coastal Engineering, ASCE, -, 1996, pp. 465–478.
[41] E. Bretherton, C. Garret, Wavetrains in inhomogeneous moving media, Proc. Roy. Soc. Lond. Ser. A 302 (1969) 529–554.
[42] N. Guillou, Evaluation of wave energy in the Sea of Iroise with two spectral models, Ocean Engineering 106 (2015) 141–151.
[43] K. Hasselmann, T. Barnett, E. Bouws, H. Carlson, D. Cartwright, K. Ende, J. Ewing, H. Gienapp, D. Hasselmann, P. Kruseman, A. Meerburg, P. Muller, D. Olbers, K. Richter, W. Sell, H. Waldden, Measurements of wind-wave growth and swell decay during the JOint North Sea WAve Project (JONSWAP), Dtsch. Hydrogr. Z. Suppl. 12 (A8) (1973) 1–95.
[44] G. Komen, S. Hasselmann, K. Hasselmann, On the existence of a fully developed wind-sea spectrum, Journal of Physical Oceanography 14 (1984) 1271–1285.
[45] A. van der Westhuysen, M. Zijlema, J. Battjes, Nonlinear saturation based whitecapping dissipation in SWAN for deep and shallow water, Coastal Engineering 54 (2007) 151–170.
[46] A. van der Westhuysen, Spectral modeling of wave dissipation on negative current gradients, Coastal Engineering 68 (2012) 17–30.
[47] P. Esposito, Résolution bidimensionnelle des équations de transport par la méthode des caractéristiques, Tech. rep.
[48] J. Smagorinsky, General circulation experiments with the primitive equations I: the basic experiments, Mon. Weather Rev. 91 (1963) 99–164.
[49] B. Quetin, Modèles mathématiques de calcul des écoulements induits par le vent, in: 17éme congrès de l'AIRH, Baden-Baden, 1977.
[50] W. Munk, E. Anderson, Notes on a theory of the thermocline, Journal of Marine Research 3 (1) (1948) 276–295.
[51] R. Flather, Results from surge prediction model of the North-West European continental shelf from April, November and December 1973, Tech. Rep. Report number 24, Institute of Oceanographic (1976).
[52] O. Philipps, The dynamics of upper ocean, Cambridge University Press, Cambridge, 1977.
[53] J. Warner, C. Sherwood, R. Signell, C. Harris, H. Arango, Development of a three-dimensional, regional, coupled wave, current, and sediment-transport model, Computers and Geosciences 34 (10) (2008) 1284–1306.
[54] R. Signell, R. Beardsley, H. Graber, A. Capotondi, Effect of wave-current interaction on wind-driven circulation in narrow, shallow embayments, Journal of Geophysical Research 95 (1990) 9671–9678.
[55] L. Quartapelle, Numerical solution of the incompressible Navier-Stokes equations, -, Birkhäuser, Berlin, 2007.
[56] T. Blackmore, L. Myers, A. Bahaj, Effects of turbulence on tidal turbines: Implications to performance, blade loads, and condition monitoring, International Journal of Marine Energy 14 (2016)

1–26.
[57] B. Loubrieu, J. Bourillet, E. Moussat, Bathy-morphologique régionale du Golfe de Gascogne et de la Manche, modèle numérique, Tech. rep., Ifremer (2008).
[58] L. Louvart, C. Grateau, The Litto3D project, in: Oceans 2005 - Europe, Brest, France, 2005.
[59] Saha et al., The NCEP climate forecast system version 2, Journal of Climate 27 (2014) 2185–2208.
[60] F. Ardhuin, IOWAGA project, https://wwz.ifremer.fr/iowaga/ (2016).
[61] N. Guillou, G. Chapalain, E. Duvieilbourg, Sea surface temperature modelling in the Sea of Iroise: assessment of boundary conditions, Ocean Dynamics 63 (2013) 849–863.
[62] A. Hamdi, M. Vasquez, J. Populus, Cartographie des habitats physiques Eunis - Côtes de France, Technical Report DYNECO/AG/10-26/JP, Ifremer (2010).
[63] R. Soulsby, The bottom boundary layer of shelf seas, in: B. E. Johns (Ed.), Physical Oceanography of Coastal and Shelf Seas, Elsevier, Amsterdam, 1983, pp. 189–266.
[64] G. Egbert, A. Bennett, M. Foreman, TOPEX/POSEIDON tides estimated using a global inverse model, Journal of Geophysical Research 99 (1994) 24821–24852.
[65] C. Willmott, On the validation of models, Physical Geography 2 (2) (1981) 219–232.
[66] E. Boudière, C. Maisondieu, F. Ardhuin, M. Accensi, L. Pineau-Guillou, J. Lepesqueur, A suitable metocean hindcast database for the design of marine energy converters, International Journal of Marine Energy 3-4 (2013) 40–52.
[67] N. Rascle, F. Ardhuin, A global wave parameter database for geophysical applications. part 2: Model validation with improved source term parameterization, Ocean Modelling 70 (2013) 174–188.